Atomic Spectroscopy

Article

Accurate analysis of Fe isotopes in Fe- dominated minerals by excimer laser ablation MC-ICP-MS on wet plasma conditions

Kaiyun Chen, Honglin Yuan,* Zhi'an Bao, and Nan Lv

State Key Laboratory of Continental Dynamics, Department of Geology, Northwest University, Xi'an, 710069

Received: *July 05, 2021;* ***Revised:*** *July 24, 2021;* ***Accepted:*** *July 24, 2021;* ***Available online:*** *July 31, 2021.*

DOI: 10.46770/AS.2021.703

ABSTRACT: The Fe isotope ratios can be a useful tracer of geochemistry, biogeochemistry, and the environmental redox state. In this study, we investigated the feasibility of Fe isotopic analysis in Fe-dominated minerals by 193 nm excimer ns laser ablation combined with Nu Plasma 1700 high resolution MC-ICP-MS without matrix-match calibration. Several important instrument parameters were investigated, such as the effect of the addition of nitrogen gas and water vapor, the effects of analytical parameters such as ablation mode, laser fluence, pulse repetition rate, spot size on Fe isotopic mass bias during analysis were investigated as well. The results showed that the effects of ablation mode, spot size, laser pulse repetition rate, and line scan speed can be neglected, while laser fluence and matrix effects had significant influence on the Fe isotopic mass bias at dry plasma condition. These problems can be minimized using consistent lower fluence (1.5–3.5 J·cm^{-2}), as well as the wet plasma conditions can significantly reduce the matrix effect in Fe isotopic analysis. Fortunately, with the water vapor and nitrogen gas addition after the ablation cell, an accurate and precise Fe isotope in pyrite, manganite, hematite, and chalcopyrite analysis by ns-LA-MC-ICP-MS can be achieved with non-matrix-matched calibration. The obtained accuracy and reproducibility of the *in situ* determinations of $\delta^{56}Fe_{IRMM-014}$ were both better than ± 0.10‰ (2 SD). This study indicated that there was a serious matrix effect in the Fe isotopic analysis of Fe-dominated minerals by ns- LA-MC-ICP-MS, and nitrogen gas mixed with water vapor-assisted ns- LA-MC-ICP-MS were an appealing option for the *in situ* Fe isotope analysis of Fe-dominated minerals with non-matrix-matched calibration.

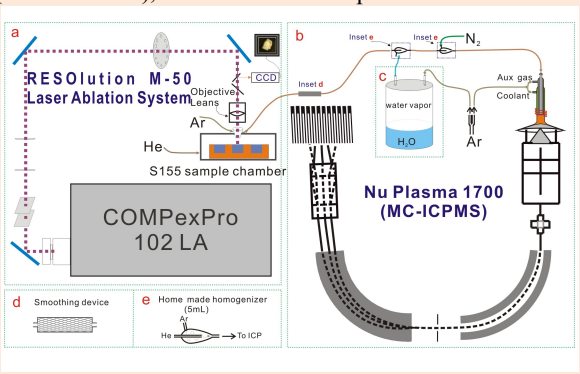

INTRODUCTION

Iron (Fe) is a transition metal element and has four stable isotopes: ^{54}Fe (5.80% of the total, atomic abundance), ^{56}Fe (91.72%), ^{57}Fe (2.20%), and ^{58}Fe (0.28%). Iron also has three valence states, Fe^0, Fe^{2+} and Fe^{3+}, which is the most important parameter controlling mass fractionation during redox reactions from inorganic and biotic processes throughout the Earth's history.[1-11] In nature, variations in the $^{56}Fe/^{54}Fe$ ratios of ~ 6‰ are observed.[8,12] The Fe-dominated minerals (pyrite, hematite, magnetite, chalcopyrite and so on), which can be found in many kinds of sedimentary, and metamorphic rocks and various deposits,[12-18] they are robust minerals associated with the processes of hydrothermal, mineralization, and metamorphism.[19] For example, pyrite is the most thermodynamically stable iron sulfide mineral near the Earth's surface.[20-22] The Fe isotope ratios of pyrite can be a useful tracer of Fe biogeochemistry[20,23] and the environmental redox state.[24,15] However, most studies have been carried out using solution nebulization multi-collector inductively coupled plasma mass spectrometry (SN-MC-ICP-MS) after sample dissolution and chemical purification with chromatography.[25-29] However, the rock minerals that might not reach isotope equilibrium or have complex structure, so the bulk analysis generally reflect a mixed signature of various endmembers, which cannot provide valuable geological information and accurately reflect isotopic changes on the micron scale.

Recently, *in situ* measurements of stable Fe isotopes have been

performed with two analytical methods: secondary ion mass spectrometry (SIMS) and laser ablation (LA) MC-ICP-MS. SIMS analysis of some high symmetry minerals results in a significant instrumental mass bias that is a function of the angle between the primary ion beam and the crystal lattice.[30-32] For example, Fe isotopes can be artificially fractionated by ~1‰ in $^{56}Fe/^{54}Fe$ and is a function of the crystal orientation of magnetite (Fe_3O_4) with respect to the primary ion beam.[32] Furthermore, the method is limited by a large matrix effect.[33,34] The precision and reproducibility of Fe isotopes from various reference materials measured by SIMS is typically 0.2‰–0.3‰ (2 SD) ,[32,34,35] while LA-MC-ICP-MS techniques provide a powerful tool for analyzing geological samples of a small sizes (*e.g.*, mineral grains, inclusions) or complex texture. Other advantages of LA-MC-ICP-MS include minimal of sample preparation and short analytical time because the sample is at ground potential and is in an inert gas atmosphere.[36] There have been significant advances in Fe isotope analysis since the pioneering work of Hirata and Ohno[37] and Hirata *et al*.[38] when the external precision of the measurements less than 0.3‰ (2 SD). Hirata and Kon[39] used a newly developed femtosecond (fs, 10^{-15}s) LA-MC-ICP-MS technique, which allowed *in situ* measurements of Fe isotopic ratios of pyrite at a spatial resolution of ~ 40 μm and precision of $^{56}Fe/^{54}Fe \pm 0.30‰$ (2 SD, n = 10). The obtained reproducibility of $\delta^{56}Fe_{IRMM-014}$ was reduced further to 0.2‰ (2 SD) by Kosler *et al*.[40], Horn *et al*.[41] and Steinhoefel *et al*.[42] published preliminary studies demonstrating the feasibility of using fs LA-MC-ICP-MS for the precise and accurate determination of Fe isotopic compositions of natural materials; their precision and accuracy of $\delta^{56}Fe$ were both better than ± 0.1‰ (2 SD). Oeser *et al*.[43] demonstrated that the reproducibility of $\delta^{56}Fe$ values determined for a certain sample relative to a laser ablated reference material (RM) was better than ± 0.12‰ (2 SD) based on a nickel standard dopping technique.

The main difficulties with high precise and accurate measurements of Fe isotope ratios using LA-MC-ICP-MS are spectrometric interference, matrix effects, laser induced isotopic mass fractionation and instrumental mass bias. A major obstacle arises from the fractionation of elemental or isotopic ratios during ablation and analysis, such as nanosecond (ns, 10^{-9} s) Nd: YAG or excimer laser ablation systems (ns-LA), which directly relate to thermal ablation generated by the interaction of ns laser pulses with the sample[41] and large particle size distributions that cause laser ablation induced isotopic fractionation.[36] This isotopic fractionation makes it difficult to achieve the high precision needed for today's applications; however, ns-laser systems can provide stoichiometric sampling under appropriate conditions. Some strategies have been developed to obtain reliable data using ns LA-MC-ICP-MS,[44] validating the possibility of using a ns-laser system for *in situ* stable Fe isotope analysis.[36] The technique has been developed to avoid interference by using high mass resolution sector field mass spectrometry, where polyatomic ion interferences can be separated in Fe determination.[26,45] An alternative approach to calibrate instrumental mass bias in LA-MC-ICP-MS is calibrator –sample -bracketing (CSB), which requires an appropriately matrix matched standard, particularly for the ns laser. Commonly employed LA systems require a standard with a similar matrix to the material under investigation. Hu Z-c *et al.*[46] indicate that the addition of nitrogen to the central gas flow in laser ablation MC-ICP-MS not only increase the sensitivity of Hf but also suppress mass fractionation. Oeser *et al.*,[47] Schuessler and von Blanckenburg,[48] Luo *et al.*,[49] and Lin *et al.*[50] applied wet plasma conditions to measure the Mg, Fe, Si and Li isotopic ratio accurately and precisely with non-matrix-matched calibration. Zheng *et al.*[51] have evaluated the matrix effects during Fe isotope analysis using a 266 nm fs laser and a 193 nm ns laser coupled to a MC-ICP-MS, found that the matrix effects during fs-LA analysis can be almost completely suppressed by introduction of water, while matrix effects during Fe isotope analysis by ns-LA result cannot be effectively suppressed by water, matrix-matching is essential during in situ Fe isotope analysis by ns-LA.

In this study, the small amount water vapor and nitrogen gas will combined add in aerosol to investigate the matrix effect on the accuracy the Fe isotope measurement by ns LA-MC-ICP-MS, and the effects of laser fluence (laser energy/spot area), ablation mode, pulse repetition rates, spot size on Fe isotopic fractionation were investigated as well. We propose accuracy *in situ* determination of Fe isotopes in Fe-dominated minerals (pyrite, chalcopyrite, magnetite and hematite) associated with excimer ns laser ablation coupled to true mass high-resolution MC-ICP-MS at the center of Fe mass-peaks instead of pseudo high resolution which measured on the shoulder of that, we optimized the laser ablation and mass spectrometry parameters to improve performance and to establish utility method for *in situ* Fe isotopic analysis.

EXPERIMENTAL

Instrumentation and analytical procedures. The instruments used in this study are a large dispersion high-resolution Nu Plasma 1700™ plasma source multi-collector ICP-MS (Nu Instruments, Wrexham, UK) and an excimer laser ablation system RESOlution-LR (Australia Scientific Instruments, Inc., Australian), set up in the State Key Laboratory of Continental Dynamics (Northwest University, China). The Nu Plasma 1700 has a unique geometry that allows resolutions above 5,000 (true mass resolution (TMR = M/ΔM, 10% valley) while maintaining a flat top peak for high precision and accurate simultaneous isotopic measurements. Each of the 16 Faraday cup collectors use 10^{11} Ω resistors and a fixed array of 10 Faraday collectors with an additional six adjustable position Faraday collectors at the low and high mass ends. The collectors possessing independently variable high-resolution slits, allowing for different resolutions on individual detectors. The instrumental resolution can be tuned using three independently adjustable slits (source slit, alpha / beta slits, and collector slits) to

Table 1 Instrumental parameters for Fe isotope measurements.

Nu Plasma 1700 MC-ICP-MS work conditions	
Coolant gas	13 L·min^{-1} Ar
Auxiliary gas	0.8 L·min^{-1} Ar
Nebulizer gas	0.8–0.9 L·min^{-1} Ar
RF power	1300 W
Accelerate voltage	6000 V
Sampling cone	Ni orifice, 1.15 mm diameter
Skimmer cone	Ni orifice, 0.6 mm diameter
Amplifier	10^{11} Ω
Faraday cup setup	L5:^{53}Cr, L4:^{54}Fe, Ax:^{56}Fe, H3:^{57}Fe, H5:^{58}Fe
Integration time	50- 60 s
Background	30 s on peak zero
RESOlution-LR M-50 Laser ablation system	
Wavelength	193 nm
pulse-width	20 ns
Fluence	1–30 J·cm^{-2}
Repetition rate	1–10 Hz
Spot size	9–380 μm
Carrier gas	0.3 L·min^{-1} He

achieve different mass resolutions for each collector. The RESOlution-LR is a 193 nm ArF excimer laser ablation system, based on the Coherent COMPexPro 193 nm excimer laser with a pulse width of 20 ns. The system permits a controlled repetition rate between 1 and 20 Hz, the laser spot size is controlled using a motorized 20-position aperture wheel with predefined sizes (diameter 9–380 μm), and the fluence is adjustable from 1 J·cm^{-2} to 30 J·cm^{-2}. The system is equipped with a *Laurin Technic* two volume sample cell S155 which have 2700mL capacity. The Faraday cup configurations for Fe isotope analysis and the instrumental parameters of MC-ICP-MS and laser ablation system used in this study are presented in Table 1.

During the Fe isotope measurements, the detector array of the Faraday cups was positioned for the simultaneous detection of ^{53}Cr, ^{54}(Fe+Cr), ^{56}Fe, ^{57}Fe, ^{58}(Fe+Ni) (Table 1). ^{53}Cr was monitored to correct for trace amount of the possible isobaric interference of ^{54}Cr on ^{54}Fe by assuming a ^{54}Cr/^{53}Cr ratio of 0.2571.[52] The instrumental drift and mass bias were corrected using the standard-sample-bracketing (SSB) technique. The dry plasma conditions achieved by the laser ablation sample introduction technique results in a smaller contribution of the mass spectrometric interference of polyatomic ions such as $[^{40}Ar^{14}N]^+$ on $^{54}Fe^+$, $[^{40}Ar^{16}O]^+$ on $^{56}Fe^+$, $[^{40}Ar^{16}O^1H]^+$ on $^{57}Fe^+$ and $[^{40}Ar^{18}O]^+$ on $^{58}Fe^+$ (Table S1). The Fe ions of interest can be completely separated from most of the interfering polyatomic ions if the required true mass resolution (TMR) is lower than 3,000. To separate the Fe ions from the interferences, the mass resolution was set above 14,000 resolving power (RP) where RP= M/ΔM (5%-95% peak side width), corresponding to ~3500 TMR (Fig. S1) by adjusting the source slit, alpha slit and collector slits, so the ion transmission relative to that at low mass resolution is about 20%. However, isobaric ions such as $^{54}Cr^+$ and $^{58}Ni^+$ could not be separated because they require an extremely high mass resolution (> 27,000 TMR) that cannot be achieved by MC-ICP-MS at present.

During solution analysis, the mass spectrometer was set in static mode, and the standard and sample solutions were diluted to 2.5 μg·mL^{-1} for wet plasma using ultrapure 2% HNO_3. The washing time used prior to each analysis was 140 s (70 s + 70 s for two 2% HNO_3 solutions) with the sampling delay and stability time totaling 90 s and 10 s the integration time for each measurement. Data acquisition was performed in three blocks of 10 measurements, and ~10 min was required for one analysis. The signal of $^{56}Fe^+$ occurred around 20 V. More details for chemical separation and solution nebulizer analysis are found in Chen *et al.*[53]

For laser ablation measurements, the time-resolved analysis (TRA) mode was used. The data acquisition strategy was 30 s on mass-peak zero for gas -blank (background) with the laser switched off, 50–60 s for the LA signal after the laser was turned on, and 30 s for washout of the previous ablation aerosols; the total acquisition time for each analysis was 120 s, and the dwell time was 0.2 s per datum. Sample aerosols were transferred to the ICP-MS by 4 mm OD high-purity Nylon tubing, and high-purity (99.9995%) He (0.300 L·min^{-1}) mixed with high-purity Ar (0.85–0.95 L·min^{-1}) for the carrier gas. The gas blanks of masses on 56 and 54 were ~0.80 mV and ~0.04 mV, respectively. The gas blanks were corrected by on-peak baseline subtraction. A novel "wave" signal-smoothing device was used for the LA-MC-ICP-MS analysis[54]. The analyzed internal precisions of relative standard errors (RSEs) were better than 0.004% for ^{57}Fe/^{54}Fe and 0.005% for ^{56}Fe/^{54}Fe. The TRA data were calculated by the Nu plasma software. Instrumental mass biases, including laser induced mass fractionation and drift of the ^{56}Fe/^{54}Fe and ^{57}Fe/^{54}Fe ratios were corrected by standard-sample-bracketing (SSB) in each LA-MC-ICP-MS analytical session by regularly analyzing specific pyrites (LY and Aa018, see below for more details) as RM throughout each analytical session.

Small volume of water vapor and nitrogen gas was added to the carrier gas before or after ablation cell, the mixed aerosol was transport with 4mm OD Nylon tube, Ultrapure water produced by using a Milli-Q water purification system (Millipore, Billerica MA, USA) was introduced into the ICP with a constant stream of argon (0.3-0.9 L min^{-1} flow rate) gas thorough the homemade quartz glass spray chamber after and before the ablation cell (Fig. 1). The calculated introduction rate of water was varying with the flow rate of argon gas. The Fe signal stability is not affected by the addition of water, but the Fe signal intensity is varying with the flow rate of

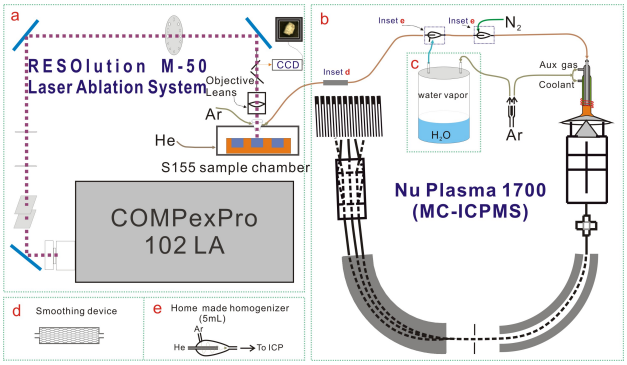

Fig. 1 Schematic diagram of instrument setup. (a) the laser ablation system RESOlution-LR M-50 with S155 sample chamber, (b) the Nu Plasma 1700 MC-ICPMS for Fe isotope analysis, (c) homemade quartz water vapor generator, (d) Smoothing device, and (e) homemade quartz homogenizer. Both He and Ar were controlled by mass flow controllers.

water vapor and nitrogen gas. The uptake rate of water vapor was calculated by weight consumption of water.

Standard and the Fe isotopic reference minerals. The standard IRMM-014 is commonly used as an international Fe isotopic reference; it is a batch of 99.9% pure Fe metal wire distributed by the Institute for Reference Materials and Measurements of the European Commission (IRMM). IRMM-014 has a homogeneous isotopic composition and a $^{56}Fe/^{54}Fe$ certified ratio of 15.6986[55].The final Fe isotope ratios are expressed as delta notation, $\delta^{56}Fe_{IRMM\text{-}014}$:

$$\delta^{56}Fe_{std}(‰) = \left[\frac{\left(\frac{^{56}Fe}{^{54}Fe}\right)_{sam}}{\left(\frac{^{56}Fe}{^{54}Fe}\right)_{std}} - 1\right] \times 1000 \qquad \text{(Eq. 1)}$$

Where std and sam represent the standard IRMM-014 and the sample, respectively.

During the laser ablation analysis, the results represent the Fe isotope ratios relative to the RM (Aa018 pyrite were used as calibrator for most measurements, and LY pyrite used RM for Aa018), while the corrected Fe isotopic ratios relative to IRMM-014 can be calculated with equation (1) and expressed as equation (2):

$$\delta^{56}Fe_{sam-std}(‰) = \frac{\delta^{56}Fe_{sam-rm} \times \delta^{56}Fe_{rm-std}}{1000} + \delta^{56}Fe_{sam-rm} + \delta^{56}Fe_{rm-std} \qquad \text{(Eq. 2)}$$

where rm represents reference material, $\delta^{56}Fe_{sam\text{-}rm}$ represents the Fe isotopic ratios of samples relative to the RM by laser ablation and $\delta^{56}Fe_{rm\text{-}std}$ indicates the Fe isotopic ratios of RM relative to the standard measured by solution nebulizer MC-ICP-MS.

The isotopic mass fractionation and accuracy for *in situ* laser ablation analysis can be expressed as $\Delta\delta^{56}Fe$ or $\Delta^{56}Fe$, the difference between two $\delta^{56}Fe$ values, A and B, A represents the LA result and B represents the solution result, expressed by $\Delta^{56}Fe_{A-B}$ in this study:

$$\Delta^{56}Fe_{A-B} = \delta^{56}Fe_A - \delta^{56}Fe_B \qquad \text{(Eq. 3)}$$

We selected five pyrite minerals for Fe isotope analysis and measured their homogeneity: 1308 pyrite (Py1308, 20 g, 10×8×5 mm cubic crystal) from Guangdong Province, CB pyrite (5 g, 200-400μm idiomorphic granular) from the Changba Pb-Zn deposit (Gansu Province), Aa018 pyrite (37 g,15×15×10 mm cubic crystal) from Navarra (Spanish), Py41 pyrite (80g, 42×31×25 mm cubic crystal) from Yunnan Province, LY pyrite (80 g, 26×18×34 mm cubic crystal) from Liyang (Hunan Province), and Py_Bal-4-13Bt,[51] magnetite Mgt08BI-12,[51] specularite Spc, hematites 6416 (Hem6416) and 6410 (Hem6410), and chalcopyrite 2656 (Ccp2656). All the samples and standards were mounted in epoxy resin and polished with 1 μm diamond paste for laser ablation analysis. Electron microprobe analysis (EMPA) (Table S2) and Energy Dispersive System (EDS) analysis (Fig. S2) indicated that most minerals were nearly chemically pure end members and major element homogenous. Iron isotope homogeneity of each mineral was confirmed by multiple single-grain analyses using conventional solution nebulization MC-ICP-MS after chromatographic purification. The $^{56}Fe/^{54}Fe$ isotopic ratios were measured in nine Fe-dominated minerals samples by solution nebulizer MC-ICP-MS firstly, all Fe isotopic data for pyrites and other Fe-dominated minerals are summarized in Table 2.

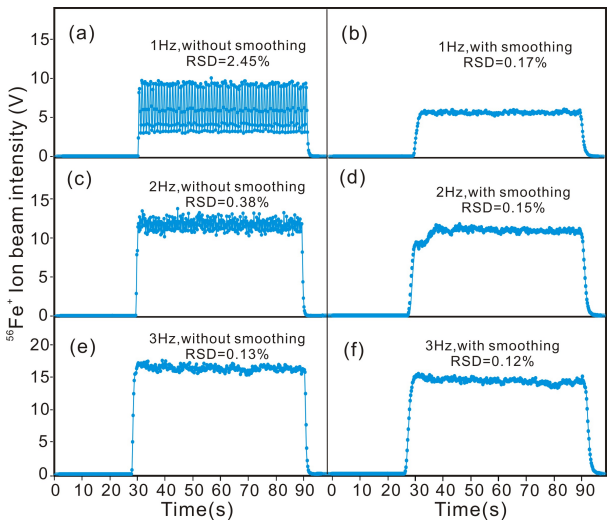

Fig. 2 The acquisition $^{56}Fe^+$ ion beam signals with and without a smoothing device. (a) 1 Hz repetition rate, without smoothing. (b) 1 Hz repetition rate, with smoothing. (c) 2 Hz repetition rate, without smoothing. (d) 2 Hz repetition rate, with smoothing. (e) 3 Hz repetition rate, without smoothing. (f) 3 Hz repetition rate, with smoothing. Analytical parameters were: laser fluence of 3.0 J·cm^{-2}, circle spot size of 13 μm, and line scan speed of 2 μm·s^{-1}. The relative standard deviations (RSDs) were calculated by standard deviations divided as the average ion beam intensities of integrated net signals (removing the gas blank) with the laser switched on.

Table 2. The Fe Isotopic Composition of Fe-rich Samples Measured by Solution nebulization and Laser Ablation MC-ICP-MS

		LA result						Solution result					
Sample	Material	$\delta^{56}Fe_{IRMM-014}$ (‰)$_{corr}$[a]	2sd[b]	$\delta^{57}Fe_{IRMM-014}$ (‰)$_{corr}$	2sd	n	MSWD	$\delta^{56}Fe_{IRMM-014}$ (‰)	2sd	$\delta^{57}Fe_{IRMM-014}$ (‰)	2sd	n	Ref.[c]
IRMM-014	Fe-metal	0.00	0.10	0.00	0.17	7		-0.00	0.05	-0.01	0.06	35	
Py1308	pyrite	0.28	0.28	0.42	0.37	115	3.6	0.36	0.04	0.52	0.06	6	
CB	pyrite	-0.96	0.07	-1.41	0.14	140	1.1	-0.89	0.04	-1.28	0.06	7	
Aa018	pyrite	0.49	0.10	0.72	0.15	189	1.1	0.52	0.04	0.73	0.05	13	
Py41	pyrite	-0.35	0.48	-0.52	0.51	95	16	-0.16	0.03	-0.26	0.07	6	
LY	pyrite	0.64	0.08	0.94	0.14	266	0.8	0.60	0.05	0.85	0.06	19	
Py_Bal-4-13B	pyrite	-1.39	0.11	-2.04	0.14	24		-1.38	0.07	-2.01	0.11	31	[51]
Spc	specularite	0.07	0.28	0.11	0.38	33	6.6	0.00	0.04	-0.04	0.04	6	
Hem6416	hematite	0.21	0.56	0.32	0.80	32	10	0.25	0.03	0.35	0.04	9	
Hem6410	hematite	0.41	0.10	0.61	0.18	23	1.1	0.42	0.05	0.60	0.04	6	
Ccp2656	chalcopyrite	0.10	0.12	0.13	0.20	39	2.7	0.10	0.04	0.11	0.05	5	
Mgt08BI-12	magnetite	0.25	0.06	0.32	0.05	16		0.32	0.05	0.51	0.09	8	[51]
AGV-2	Andesite							0.11	0.05	0.16	0.09	6	
								0.105	0.012	0.146	0.019	7	[29]
								0.096	0.027	0.148	0.039	25	[52]
BCR-2	Basalt							0.10	0.03	0.13	0.05	6	
								0.091	0.032	0.126	0.066	9	[29]
								0.084	0.029	0.130	0.048	17	[52]
GSP-2	Granodiorite							0.15	0.03	0.22	0.07	6	
								0.159	0.038	0.230	0.047	6	[29]
								0.157	0.025	0.222	0.038	16	[52]

a. The corrected $\delta^{56}Fe_{IRMM-014}$ and $\delta^{57}Fe_{IRMM-014}$ relative to IRMM-014.
b. 2 standard deviation.
c. Ref. represent data from the reference articles.

RESULTS AND DISCUSSION

The Fe ion beam signal and stability. The stability of Fe ion beam intensities is defined as the relative standard deviation (RSD, %) of 50 s integrated sample signals after the laser was switched on and with a laser fluence of 3.0 J·cm^{-2}, 13 μm spot size (circle spot), and a line scan speed of 2 μm·s^{-1} with Aa018. The stability of Fe ion beam (*i.e* $^{56}Fe^{+}$) intensities for the sample with and without smoothing device are 0.17% and 2.45%, respectively (Fig. 2). The stabilities achieved by 2 Hz and 3 Hz without smoothing were 0.38% and 0.13%, respectively, while the stabilities achieved with smoothing were 0.15% (2 Hz) and 0.12% (3 Hz). Using the wave stabilizer improved the signal stability by more than a factor of 10 and no oscillation of the signal intensity was observed at a repetition rate of 1 Hz; however, when the laser repetition rate was greater than 3 Hz, there was no significant improvement in stability. These findings indicate that the smoothing device is very useful for low repetition rate (≤ 3 Hz) laser ablation, which provides better precision and spatial resolution[54]. The use of a smoothing device increases the washout time but remains < 2 s, so it is negligible for 60 s ablating time during Fe isotope measurements. The smoothing device was thus used in our experiment hereafter.

The Fe concentration effect on Fe isotopic analysis. A concentration effect can be seen in solution nebulizer MC-ICP-MS[25,45,57]. However, in laser ablation measurement, the Fe content in minerals cannot be changed, so the concentration effect is best described as an ion signal intensity effect, which can be explored by the relationship of isotopic mass fractionation with different ion signal intensities between samples and RM. We investigated isotopic mass fractionation changes with ion signal intensities by tuning the laser ablation parameters. During the experiment, Aa018 pyrite was used as both the RM and sample. The laser

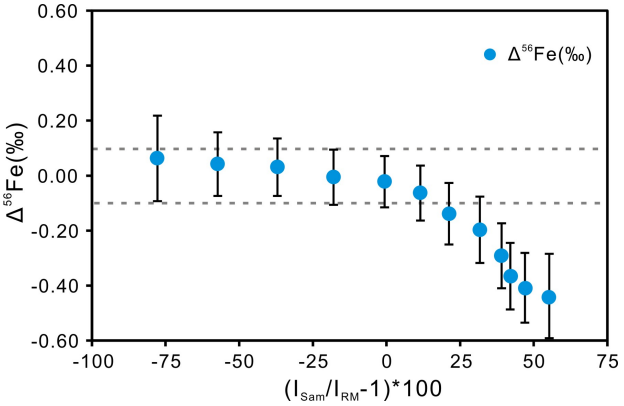

Fig. 3 Isotopic mass fractionation as a function of ion beam intensities. Here I_{Sam}/I_{RM} = intensity of sample / intensity of reference material (RM) (~24 V Fe ion intensity). The isotopic mass fractionation $\Delta^{56}Fe$ was determined as the difference between the measured $^{56}Fe/^{54}Fe$ ratios of various sample signals and RM signals. All of the $\Delta^{56}Fe$ values are relative to the same analytical parameters (laser fluence 3.0 J·cm^{-2}, line scan spot size 13 μm, scan speed 2 μm·s^{-1} and repetition rate 5 Hz). The error bars of $\Delta^{56}Fe$ are 2 standard deviations (SD) of three repeat measurements at the same analytical conditions, the dashed lines denote the typical analytical uncertainty (± 0.10‰, 2 SD) of the laser ablation analyses.

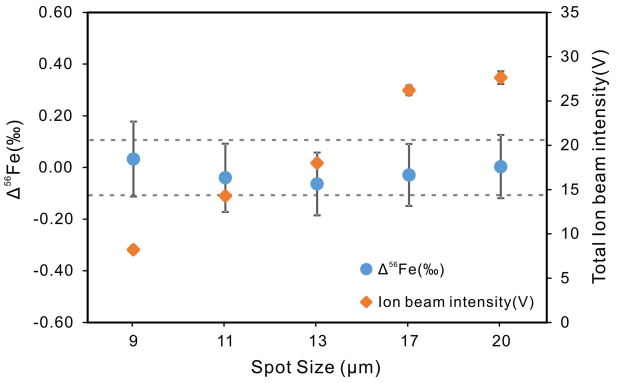

Fig. 4 The effect of laser spot size on Fe ion beam intensity and Fe isotopic mass fractionation by line scan ablation. All of the $\Delta^{56}Fe$ values were generated under the same analytical conditions (laser fluence 3.0 J·cm^{-2}, scan speed of 2 μm·s^{-1} and repetition rate 3 Hz). The error bars are 2 standard deviations of three repeat measurements, the dashed lines represent the typical analytical uncertainty (± 0.10‰, 2 SD) of the laser ablation analyses.

fluence was set to 3.0 J·cm^{-2}, the spot size was13 μm (circle), and the line scan speed was 2 μm·s^{-1} for all measurements. The laser repetition rate over a range from 1 to 11 Hz for the sample was measured against a laser repetition rate 5 Hz for the RM (the total ion beam was ~22 V). The isotopic mass fractionation bias $\Delta^{56}Fe$ varied with the intensity ratios I_{Sam}/I_{RM} (Fig. 3). There were no significant isotopic mass fractionations ($\Delta\delta^{56}Fe$ = ~0‰) when the intensity ratios I_{Sam}/I_{RM} ranged from 0.25 to 1.20, but lower intensity ratios (I_{Sam}/I_{RM} < 0.60) produced positive isotopic mass fractionations, and higher intensity ratios (I_{Sam}/I_{RM} > 1.20) gained negative isotopic mass fractionations. This indicates that a large difference in ion intensity will cause isotopic mass fractionation, so signal intensity matching is important for accurate *in situ* laser ablation Fe isotopic determination.

The line scan spot size effect on Fe isotope analysis. We used the line scan ablation method at laser fluence 3.0 J·cm^{-2}, a scan speed of 2 μm·s^{-1} and laser frequency of 3 Hz, but we changed the aperture of the spot size to study the spot size effect on Fe isotopes in pyrite with laser ablation analysis. During the experiment, the spot sizes used were 9 μm diameter (circle), 11 μm (square spot), 13 μm (circle), 17 μm (square) and 20 μm (circle). The results showed that the total Fe ion beam intensities increased from 8 to 28 V with the spot size from 9 to 20 μm and the laser fluence of 3.0 J·cm^{-2}, scan speed of 2 μm·s^{-1}, and a 3 Hz repetition rate (Fig. 4), the larger spot sizes allow for the ablation of more material and aerosols and thus achieves higher ion intensities. It seems that there are fewer isotopic mass fractionations ($\Delta\delta^{56}Fe$ closing to 0‰) at different spot size conditions when the signal intensity is matched. At the same time, the internal precision of $^{56}Fe/^{54}Fe$ acquired by the larger spot size is better than the smaller spot size because the larger spot size produced more aerosols and a higher signal intensity.

The line scan speed effect on Fe isotope analysis. We used the line scan ablation method with a circle spot size 13 μm, laser fluence of 3.0 J·cm^{-2} and laser frequency of 3 Hz while changing the line scan speed to study its effect on the Fe isotopic ratios analysis. During the experiments, the line scan speeds were changed from 1 μm·s^{-1} to 5 μm·s^{-1}. The results showed that the average Fe ion beam intensities (variation range 22–24 V) were basically consistent with each other over scan speeds range from 1 μm·s^{-1} to 5 μm·s^{-1}, and iron isotopic compositions are basically the same ($\Delta\delta^{56}Fe$ closing to 0‰) (Fig. 5). This indicates that there is no isotopic mass fractionation at different scan speed conditions,

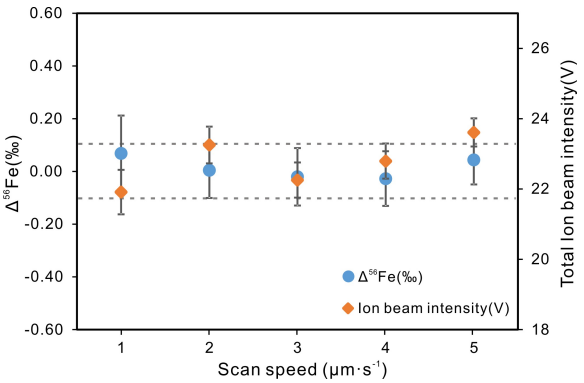

Fig. 5 The effect of laser scan speed on Fe ion beam intensity and Fe isotope ratios. Except for scan speed (1–5 μm·s^{-1}), all of the $\Delta^{56}Fe$ values were generated under the same analytical conditions (laser fluence 3.0 J·cm^{-2}, circle spot size 13 μm, and repetition rate 3 Hz). The error bars are 2 standard deviations of three repeat measurements for each data point, the dashed lines represent the typical analytical uncertainty (± 0.10‰, 2 SD).

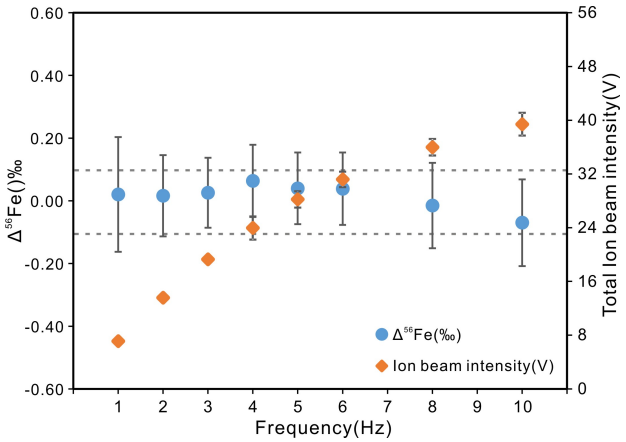

Fig. 6 The effect of laser repetition rate on Fe ion beam intensity and Fe isotope ratios. Except for repetition rate (frequency 1–10 Hz), all of the Δ^{56}Fe values were generated under the same analytical conditions (circle spot size 13 μm, laser fluence 3.0 J·cm^{-2} and line scan speed 2 μm·s^{-1}). The error bars are 2 standard deviations of three repeat measurements at least, the dashed lines represent the typical analytical uncertainty (± 0.10‰, 2 SD).

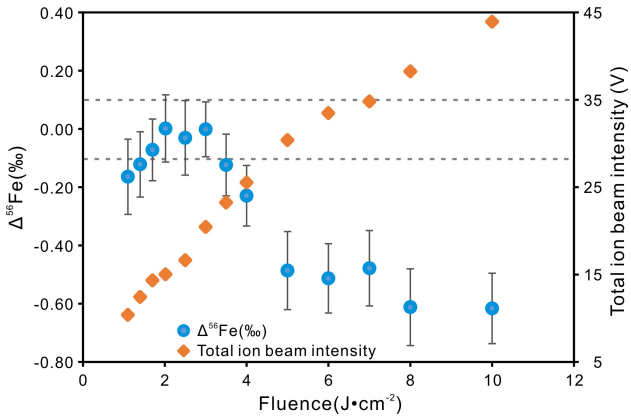

Fig. 7 The effect of laser fluence on Fe ion beam intensity and Fe isotope ratios. Except for laser fluence (1–10 J·cm^{-2}), all of the Δ^{56}Fe values were generated under the same analytical conditions (circle spot size 13 μm, laser repetition rate 3 Hz and line scan speed 2 μm·s^{-1}). The error bars are 2 standard deviations of three repeat measurements, the dashed lines represent the typical analytical uncertainty (± 0.10‰, 2 SD).

and the spatial resolution can be improved to 13 × 60 μm when the scan speed is set to 1 μm·s^{-1} for line scan mode analysis.

The laser repetition rate effect on Fe isotope analysis. We use the line scan ablation method with a circle spot size of 13 μm, laser fluence of 3.0 J·cm^{-2} and line scan speed of 2 μm·s^{-1} while changing the laser repetition rate to investigate its effect on Fe isotope. During the experiments, the laser repetition rate was varied from 1 Hz to 10 Hz. The Fe ion beam intensities are increased from 6V to 40 V when the laser repetition rates ranged from 1Hz to 10 Hz (Fig. 6), suggesting high frequency achieves high Fe ion beam intensities, and the Fe isotopic compositions are basically the same ($\Delta\delta^{56}$Fe approaching 0‰). This indicates no isotopic mass fractionation at different laser repetition rates ranging from 1 Hz to10 Hz. However, as the repetition rate increases, the depth of the ablation crater increases as well, which means the sample surface will defocus and it becomes more difficult to extract laser ablation produced aerosols out of the crater as it deepens.[40] This suggests that although Fe isotopes will have few mass fractionations with different laser repetition rates, we have higher accuracy and consistent isotopic compositions ($\Delta\delta^{56}$Fe less than ± 0.05‰) when the laser repetition rates are lower than 6 Hz.

The laser fluence effect on Fe isotope analysis. The effect of laser fluence on the Fe isotopic mass fractionation was investigated over a range of 1.0–10.0 J·cm^{-2} using the excimer laser ablation systems. We used line scan ablation mode with a circle spot size of 13 μm, laser repetition rate of 3 Hz and line scan speed of 2 μm·s^{-1} while changing the laser fluence. The results showed that the Fe ion beam intensities increased with laser fluence; high fluence achieved high ion beam intensities, and Fe isotope compositions changed with the laser fluence, the $\Delta\delta^{56}$Fe are closing to 0‰ in the case of laser fluence from 1.5 to 3.5 J·cm^{-2}, while the isotopic bias of $\Delta\delta^{56}$Fe will had an obvious negative deviation from 0‰ (more than 0.1‰) when the fluence was lower than 1.5 J·cm^{-2} and higher than 3.5 J·cm^{-2} (Fig. 7). This indicates that there are no significant isotopic mass fractionations when the fluence ranges from 1.5 to 3.5 J·cm^{-2}, but there is a distinct $\Delta\delta^{56}$Fe bias when the laser fluence is lower than 1.5 J·cm^{-2} or higher than 3.5 J·cm^{-2}. The laser fluence affects the laser ablating rate, particle morphology, size distribution, and size-dependent isotope fractionation[36,58]. When the laser fluence is lower than 1.5 J·cm^{-2}, it may be close to or less than the ablation threshold values. In contrast, when the laser fluence is higher than 3.5 J·cm^{-2}, much bigger aerosol particle sizes are ablated, which seriously affect the aerosol transmission and ionization efficiency.

The ablation method effect on Fe isotope analysis: line scan and single spot. To study the laser ablation mode effect on Fe isotopic analysis, we conducted a single spot and line scan analysis to study the effect on the Fe isotopic analysis under the same laser fluence, repetition rate and total ion signal intensity conditions. During the experiments, a laser fluence of 3.0 J·cm^{-2}, laser frequency of 3 Hz was used for both line scan and single spot by *in situ* ablation. A circle aperture spot size 13 μm and scan speed of 2 μm·s^{-1} were used for line scan ablation and achieved ~ 20 V ion beam intensity for $^{56}Fe^{+}$. To obtain the same signal intensity of the line scan mode for signal intensity matching, the spot size in single spot mode was tuned to a 17 μm diameter square adapted for the same Fe ion beam signal intensity. The ablating area was 13 ×120 μm for line scan mode, and 17 ×17 μm for single spot analysis. The Fe isotopic composition measured by line scan mode was $\Delta\delta^{56}$Fe = 0.02 ± 0.06‰ (2 SD, n = 13) which is in good agreement with the solution result within 2 SD uncertainties, while the single spot mode result $\Delta\delta^{56}$Fe = 0.07 ± 0.07‰ (2 SD, n = 13)

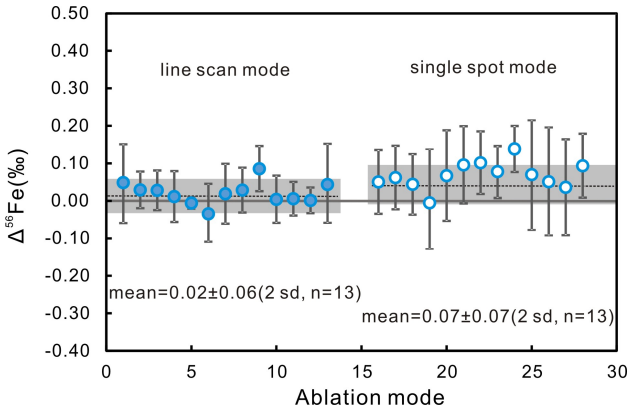

Fig. 8 The isotopic mass fractionation measured by line scan mode and single spot laser ablation analysis. The error bars are 2 standard deviations of three repeat measurements, the solid line represents the value of δ^{56}Fe measured by solution nebulizer MC-ICP-MS, the dashed line represents average values of δ^{56}Fe measured by line scan mode (left) and single spot (right) measurement, and the gray area represents the analytical uncertainty (2 SD).

is also in good agreement with the solution result in 2 SD uncertainties (Fig. 8). This indicates that both the internal and external precision and repeatability of the line scan mode is better than single spot measurements. This is because the signal and laser induced mass fractionation by a line scan is more stable, while those mass fractionation by single spot ablation changes with the ablation hole.

Matrix effects and accuracy. The solution results yielded a bulk δ^{56}Fe values of 0.36 ± 0.04‰ (2 SD) for py1308, −0.89 ± 0.04‰ (2 SD) for CB, 0.52 ± 0.04‰ (2 SD) for Aa018, −0.16 ± 0.03‰ (2 SD) for Py41, 0.60 ± 0.05‰ (2 SD) for LY, 0.00 ± 0.04‰ (2 SD) for Spc, 0.25 ± 0.03‰ (2 SD) for Hem6416, 0.42 ± 0.05‰ (2 SD) for Hem6410, and 0.10 ± 0.04‰ (2 SD) for Ccp2656 (Table 2). Where available, the Fe isotope values of the standards BCR-2, AGV-2 and GSP-2 obtained in this study by solution nebulizer MC-ICP-MS were compared with values published previously for the same reference materials by Craddoock *et al.*[29] and He *et al.*[52] There is good agreement between the Fe isotopic compositions measured by solution nebulizer MC-ICP-MS from this and the published studies within 2 SD analytical uncertainties. Three-isotope plots of Fe for the Fe-dominate minerals analyzed by LA-MC-ICP-MS are shown in Fig. 9a, data in Table 2 and yielded a slope of 1.477 ± 0.02 (2 SD, R^2 = 0.999) in a plot of δ^{57}Fe and δ^{56}Fe, which is indistinguishable within error from the equilibrium (1.475) mass-dependent fractionation law[56]. This suggests an insignificant contribution of interfering polyatomic ions to the Fe peak shoulders. Overall, the agreement between the Fe isotopic compositions of pyrite CB, Aa018, LY and Py_Bal-4-13B, hematite Hem6410, chalcopyrite Ccp2656, magnetite Mgt08BI-12 measured by LA-MC-ICP-MS and solution nebulizer MC-ICP-MS was good within 2 SD analytical uncertainty (Fig. 9b), however pyrite Py1308 and Py41, hematite Hem6416, and

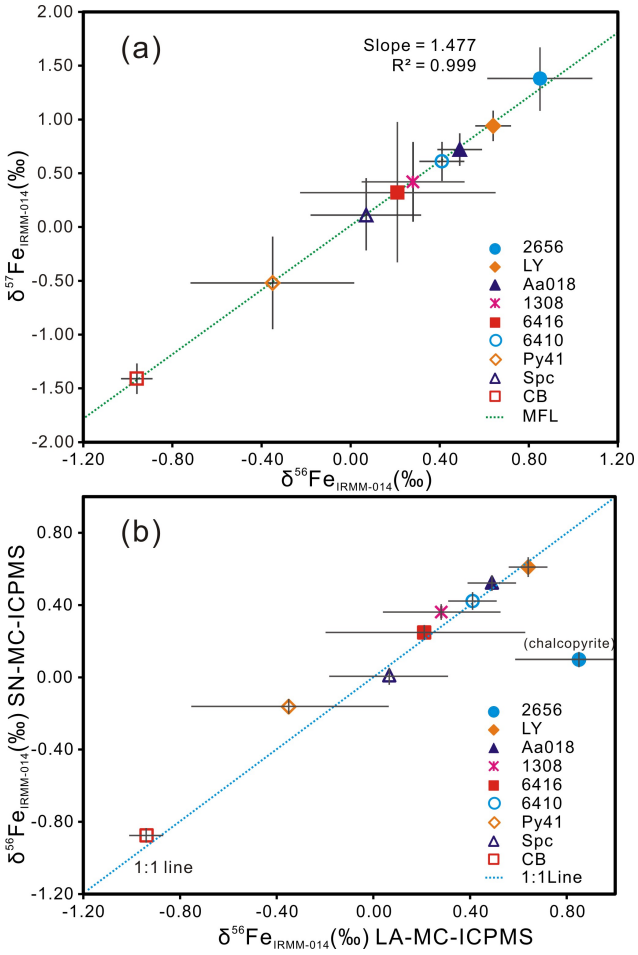

Fig. 9 (a) Three-isotope plots (δ^{56}Fe versus δ^{57}Fe) of Fe for the Fe-rich minerals analyzed by laser ablation MC-ICP-MS. (b) Comparison of δ^{56}Fe values obtained by solution nebulization (SN) MC-ICP-MS with LA-MC-ICP-MS in situ analysis. Error bars are 2 standard deviations of replicate analyses. Data are from Table 2.

specularite Spc which have an inhomogeneous iron isotopic composition. The concordance between laser ablation Fe isotopic ratios and solution nebulizer MC-ICP-MS results suggests that Fe isotopic ratios can be measured accurately at precisions better than ± 0.08‰ (2 SD uncertainties) when the sample is isotopically homogeneous.

Matrix effects between different Fe-dominate minerals were investigated by analyzing pyrite, chalcopyrite, hematite and magnetite, pyrite LY and Aa018 used as an external standard RM to correct for instrumental mass bias and isotopic mass fractionation during measurement with or without addition of nitrogen and water vapor. All minerals were analyzed with the same analytical parameters (laser fluence 3.0 J·cm^{-2}, laser repetition rate 3 Hz and line scan speed 2 μm·s^{-1}) and ion signal intensity matching by different spot sizes. Laser spot sizes were selected to give similar ^{56}Fe signal intensities (~20 V) for all mineral samples: 17 μm for LY, Aa018 and CB (pyrites), 30 μm

for Ccp2656 (chalcopyrite), and 25 μm for Hem6410 and 6416 (hematite) and Mgt08BI-12 (magnetite)[51]. Aa018 (LY was used for Aa018 calibrate) pyrite used as calibrator to correct instrumental mass bias and isotopic mass fractionation. With pyrite LY or Aa018 as the calibration standard, the δ^{56}Fe values of the four iron-dominated minerals were repeatedly analyzed by ns-LA-MC-ICP-MS with line scan mode, which yielded good measurement reproducibility, such as a 2SD of 0.08‰, 0.10‰, 0.07‰, 0.12‰, 0.10‰ and 0.06‰ for LY, Aa018 and CB, Ccp2656, Hem6410 and Mgt08BI-12, respectively. The laser ablation results without addition of nitrogen or water yielded *in situ* δ^{56}Fe values of 0.85 ± 0.29‰ (2 SD, n = 39) for Ccp2656, 0.07 ± 0.28‰ (2 SD, n = 33) for Spc, 0.41 ± 0.10‰ (2 SD, n = 23) for Hem6410, and 0.21 ± 0.56‰ (2 SD, n = 32) for Hem6416 (Fig. 9a). The accuracy of $\Delta\delta^{56}$Fe (‰), the degree of the matrix effect was determined as the difference between the laser ablation result and the solution values ("true values", measured by solution nebulizer MC-ICP-MS, Table 2) for the reference mineral (Fig. 9a). The $\Delta\delta^{56}$Fe for Spc is 0.07‰, the $\Delta\delta^{56}$Fe for Hem6410 is -0.01‰, the $\Delta\delta^{56}$Fe for Hem6416 is -0.04‰, and the $\Delta\delta^{56}$Fe for Ccp2656 is 0.75‰. The measured Fe isotope ratios, and Hem6410 and Hem6416 showed a small negative deviation relative to the pyrites (Aa018, LY and CB), while the measured Fe isotope ratios for Ccp2656 showed a large positive deviation. There are significant matrix effects for chalcopyrite, but none for the specularite and hematite with the 193 nm excimer laser ablation, indicating that the matrix effects are mineral dependent. Ablation crater SEM images (Fig. S3) show that the IRMM-014 has a serious melting edge and the amount of ablated material is very large; the chalcopyrite also has a melting edge, but the pyrite craters have sharpness of border, and the amount of ablated material is very small, there is no obvious melting phenomenon. As reported by previous studies[36,44,51], many particle sizes larger than 0.1 μm are ablated by a ns excimer laser, which have shown that the particle size distribution varies with the mineral species. Therefore, the particle size distribution for various minerals will result in different aerosol transmission and ionization efficiency and produce different isotopic mass fractionations. Thus, it is necessary to matrix match during ns laser ablation MC-ICP-MS analysis without addition of water vapor or nitrogen gas.

After added of nitrogen gas or water vapor before the sample ablation cell, the achieved Fe signal intensity and isotopic ratios change with time due to the large volume of the ablation cell (up to 2700 mL), so we did not do that in the later experiments. After addition of nitrogen gas after the sample ablation cell, the obtained iron isotopic $\Delta\delta^{56}$Fe values varies with the nitrogen flow rate. The $\Delta\delta^{56}$Fe values of pyrite is stable and agree with solution result when the flow rate of N_2 is 1-2 mL·min^{-1}, when the flow rate is 3 mL·min^{-1}, the $\Delta\delta^{56}$Fe values of pyrite have a negative deviation of -0.85‰. The $\Delta\delta^{56}$Fe values of magnetite have a negative deviation when the flow rate of N_2 is 0-1 mL·min^{-1}, but they are agreement with solution result in 2SD uncertainties (0.08%) when the flow

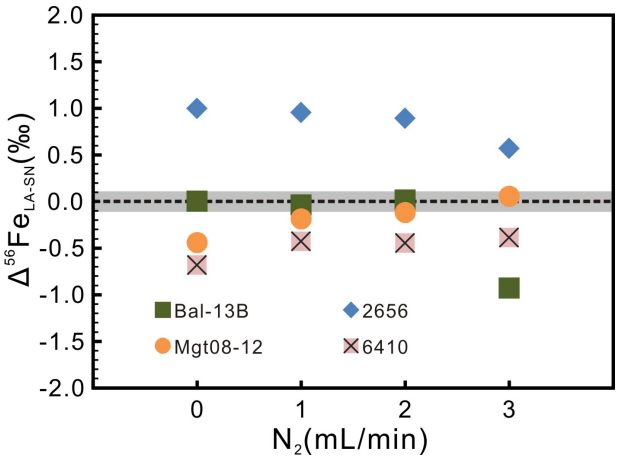

Fig. 10 Fe isotope matrix effects of different Fe-rich minerals analyzed by laser ablation MC-ICP-MS with addation of N_2. The Δ^{56}Fe value is the difference between laser ablation results and solution values. All of the Δ^{56}Fe values were generated under the same analytical conditions (laser fluence 3.0 J·cm^{-2}, laser repetition rate 3 Hz and line scan speed 1 μm·s^{-1}) and ion signal intensity matching. The error bars are 2 standard deviations of replicate measurements (n ≥10), and the dashed lines represent the typical analytical uncertainty (± 0.10‰, 2 SD).

rate of N_2 is 2-3 mL·min^{-1}. The obtained $\Delta\delta^{56}$Fe values of hematite and chalcopyrite are always have small deviations, they are closer to zero (δ^{56}Fe closer to the solution value) with the increase of nitrogen flow rate (Fig. 10). So, the addition of nitrogen gas will significantly reduce the matrix effect of pyrite, magnetite, hematite and chalcopyrite, and obtained high precision and accuracy Fe isotopic data without matrix matched calibration except hematite and chalcopyrite.

After added of water vapor after the sample ablation cell, the obtained iron isotope ratio $\Delta\delta^{56}$Fe values varies with the nitrogen flow rate. The $\Delta\delta^{56}$Fe values of pyrite is small than ±0.05‰, they are stable and agreement with solution result when the uptake rate of water vapor less than 20 μg·min^{-1}(Fig. 11). The $\Delta\delta^{56}$Fe values of magnetite have a small deviation (<±0.05‰) when the uptake rate of water vapor is 5-10 μg·min^{-1}. The obtained $\Delta\delta^{56}$Fe values of hematite and chalcopyrite are always have deviations, but they are closer to zero (closer to the true value) with the uptake rate of water vapor is 10-20 μg·min^{-1}. So, the addition of water vapor will significantly reduce the matrix effect of pyrite, magnetite, hematite and chalcopyrite, and obtained high precision and accuracy Fe isotopic data without matrix matched calibration except hematite and chalcopyrite.

After added of water vapor and nitrogen gas after the sample ablation cell, the obtained iron isotope ratio $\Delta\delta^{56}$Fe values varies with the nitrogen and water vapor flow rate. The $\Delta\delta^{56}$Fe values of pyrite is small than ±0.05‰, they are stable and agreement with solution result after the addition of 1-2 mL·min^{-1} N_2 and 10-20 μg·min^{-1} water vapor (Fig. 12). The $\Delta\delta^{56}$Fe values of magnetite and chalcopyrite have small deviations (<±0.05‰) after addition of 1 mL·min^{-1} N_2 and 5-15 μg·min^{-1} water vapor. The obtained

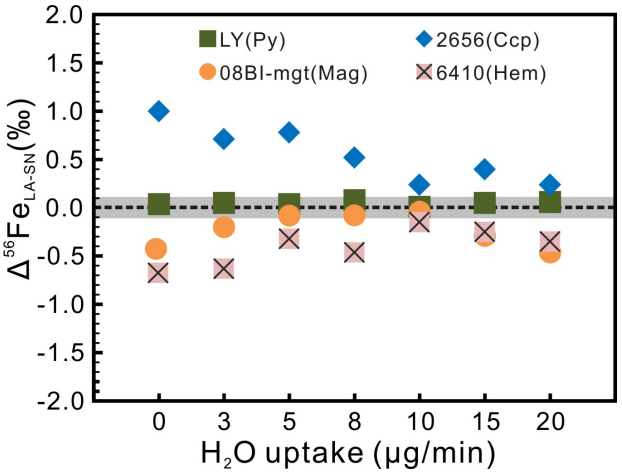

Fig. 11 Fe isotope matrix effects of different Fe-rich minerals analyzed by laser ablation MC-ICP-MS with addation of water vapor. The Δ^{56}Fe value is the difference between laser ablation results and solution values. All of the Δ^{56}Fe values were generated under the same analytical conditions (laser fluence 3.0 J·cm^{-2}, laser repetition rate 3 Hz and line scan speed 1 μm·s^{-1}) and ion signal intensity matching. The error bars are 2 standard deviations of replicate measurements (n ≥10), and the dashed lines represent the typical analytical uncertainty (± 0.10‰, 2 SD).

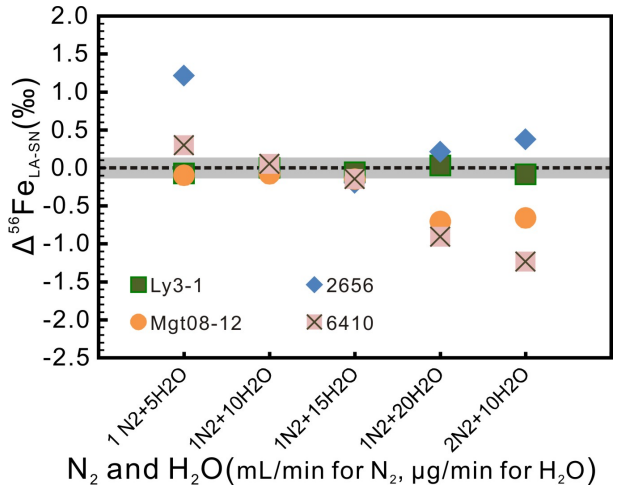

Fig. 12 Fe isotope matrix effects of different Fe-rich minerals analyzed by laser ablation MC-ICP-MS with addation of mixed N_2 and water vapor. The Δ^{56}Fe value is the difference between laser ablation results and solution values. All of the Δ^{56}Fe values were generated under the same analytical conditions (laser fluence 3.0 J·cm^{-2}, laser repetition rate 3 Hz and line scan speed 1 μm·s^{-1}) and ion signal intensity matching. The error bars are 2 standard deviations of replicate measurements (n ≥10), and the dashed lines represent the typical analytical uncertainty (± 0.10‰, 2 SD).

$\Delta\delta^{56}$Fe values of hematite have a small deviation (<±0.05‰) after addition of 1 mL·min^{-1} N_2 and 10-15 μg·min^{-1} water vapor. So, the addition of N_2 together with water vapor will significantly reduce the matrix effect of pyrite, magnetite, hematite and chalcopyrite, and obtained high precision and accuracy Fe isotopic data without matrix matched calibration after addition of 1 mL·min^{-1} N_2 and 10-15 μg·min^{-1} water vapor. Compare with previous studies,[51] the introduction of water vapor combine with nitrogen gas can significantly reduce matrix effects, reduced deviation by added of water vapor and nitrogen after the ablation cell can be regarded as the reduction of the matrix effect in the ICP ionization process and transportation process, this discovery extends the scope of excimer laser ablation analysis in the field of non-traditional stable isotopes.

CONCLUSIONS

In this study, a 193 nm excimer laser ablation system coupled with a true mass high-resolution Nu Plasma 1700 MC-ICP-MS was used to determine the Fe isotopic composition in Fe- dominated minerals. We specifically focused on the matrix effects with or without additional of water vapor and N_2 gas, and the effect of laser fluence, pulse repetition rate, spot size, and other laser parameters on the precision and accuracy of Fe isotope ratios were also systematically investigated by ns excimer laser ablation. The results showed that the effects of spot size and laser pulse repetition rate and line scan speed can be neglected, the ion signal intensity effect is not serious, while laser fluence and matrix effects have significant influence on the Fe isotopic mass fractionation; these problems can be minimized using consistently lower laser fluence (1.5–3.5 J·cm^{-2}), as well as signal intensity and matrix matching. These results demonstrate the importance of using matrix matching reference materials for Fe isotope analyses by ns LA-MC-ICP-MS with laser fluence ranges of 1.5–3.5 J·cm^{-2}. The technique is both sensitive and rapid: spot sizes as small as 13 × 60 μm for line scan and 17 μm for single spot may be readily analyzed with accuracy and high precision at a high spatial resolution. The achieved precision and accuracy are both better than ± 0.10‰ (2 SD) for $\delta^{56}Fe_{IRMM-014}$ after multiple repeat analyses of a homogeneous sample by LA-MC-ICP-MS using the instrumental configuration and laser parameters described.

For ns-LA-MC-ICPMS if use only one of the water vapor or nitrogen gas after the ablation cell, the matrix induced deviation could be reduced to a large extent, but a large deviation still existed. While, with the addition of water vapor mixed with N_2 after the ablation cell by ns-LA-MC-ICP-MS, the matrix-induced deviation (1.5%) can be suppressed, the obtained results showed excellent agreement with the SN values. Hence, for accurate Fe isotopic ratio measurements of Fe-dominated minerals, the continuous introduction of water vapor and N_2 into the plasma can support more robust conditions to realize non-matrix-matched calibration. Thus, the accurate and precise Fe isotopic composition of Fe-dominated minerals can be analyzed by LA-MC-ICP-MS with and without matrix matched calibration.

AUTHOR INFORMATION

Corresponding Author

* H. L. Yuan

Email address: yhlsklcd@126.com

Notes

The authors declare no competing financial interest.

ACKNOWLEDGMENTS

Thanks to two anonymous reviewers for their constructive suggestions. We thank Dr. Xinyuan Zheng for providing pyrite and magnetite standards. This work was co-supported by National Nature Science Foundation of China (42073051, 41421002, and 41503004) and the MOST Special Fund from the State Key Laboratory of Continental Dynamics and the Opening Foundation of the Beijing SHRIMP Center.

REFERENCES

1. B. L. Beard, C. M. Johnson, L. Cox, H. Sun, K. H. Nealson, and C. Aguilar, *Science*, 1999, **285**, 1889-1892. https://doi.org/10.1126/science.285.5435.1889
2. A. D. Anbar, *Earth Planet. Sc. Lett.*, 2004, **217**, 223-236. https://doi.org/10.1016/S0012-821X(03)00572-7
3. C. M. Johnson, B. L. Beard, E. E. Roden, D. K. Newman, and K. H. Nealson, *Rev. Mineral. Geochem.*, 2004, **55**, 359-408. https://doi.org/10.2138/gsrmg.55.1.359
4. N. Dauphas, M. van Zuilen, M. Wadhwa, A. M. Davis, B. Marty, and P. E. Janney, *Science*, 2004, **306**, 2077-2080. https://doi.org/10.1126/science.1104639
5. O. J. Rouxel, A. Bekker, and K. J. Edwards, *Science*, 2005, **307**, 1088-1091. https://doi.org/10.1126/science.1105692
6. N. Dauphas and O. Rouxel, *Mass Spectrom. Rev.*, 2006, **25**, 515-550. http://dx.doi.org/10.1002/mas.20078
7. A. D. Anbar and O. Rouxel, *Annu. Rev. Earth Pl. Sc.*, 2007, **35**, 717-746. https://doi.org/10.1146/annurev.earth.34.031405.125029
8. C. M. Johnson, B. L. Beard, and E. E. Roden, *Annu. Rev. Earth Pl. Sc.*, 2008, **36**, 457-493. https://doi.org/10.1146/annurev.earth.36.031207.124139
9. C. M. Johnson, B. L. Beard, C. Klein, N. J. Beukes, and E. E. Roden, *Geochim. Cosmochim. Ac.*, 2008, **72**, 151-169. https://doi.org/10.1016/j.gca.2007.10.013
10. J. Foden, P. A. Sossi, and C. M. Wawryk, *Lithos*, 2015, **212–215**, 32-44. https://doi.org/10.1016/j.lithos.2014.10.015
11. P. A. Sossi, O. Nebel, and J. Foden, *Earth Planet. Sc. Lett.*, 2016, **452**, 295-308. https://doi.org/10.1016/j.epsl.2016.07.032
12. K. Yoshiya, M. Nishizawa, Y. Sawaki, Y. Ueno, T. Komiya, K. Yamada, N. Yoshida, T. Hirata, H. Wada, and S. Maruyama, *Precambrian Res.*, 2012, **212–213**, 169-193. https://doi.org/10.1016/j.precamres.2012.05.003
13. Rouxel, Y. Fouquet, and J. N. Ludden, *Geochim. Cosmochim. Ac.*, 2004, **68**, 2295-2311. https://doi.org/10.1016/j.gca.2003.11.029
14. S. Graham, N. Pearson, S. Jackson, W. Griffin, and S. Y. O'Reilly, *Chem. Geol.*, 2004, **207**, 147-169. https://doi.org/10.1016/j.chemgeo.2004.02.009
15. A. Hofmann, A. Bekker, O. Rouxel, D. Rumble, and S. Master, *Earth Planet. Sc. Lett.*, 2009, **286**, 436-445. https://doi.org/10.1016/j.epsl.2009.07.008
16. M. Blanchard, F. Poitrasson, M. Méheut, M. Lazzeri, F. Mauri, and E. Balan, *Geochim. Cosmochim. Ac.*, 2009, **73**, 6565-6578. https://doi.org/10.1016/j.gca.2009.07.034
17. Y. Wang, X. -K. Zhu, J. -W. Mao, Z. -H. Li, and Y. -B. Cheng, *Ore Geol. Rev.*, 2011, **43**, 194-202. https://doi.org/10.1016/j.oregeorev.2010.12.004
18. A. Galić, P. R. D. Mason, J. M. Mogollón, M. Wolthers, P. Z. Vroon, and M. J. Whitehouse, *Chem. Geol.*, 2017, **449**, 135-146. https://doi.org/10.1016/j.chemgeo.2016.12.006
19. Q. Wang and J. W. Morse, *Mar. Chem.*, 1996, **52**, 99-121. https://doi.org/10.1016/0304-4203(95)00082-8
20. C. Archer and D. Vance, *Geology*, 2006, **34**, 153-156. https://doi.org/10.1130/G22067.1
21. J. J. Virtasalo, M. J. Whitehouse, and A. T. Kotilainen, *Geology*, 2013, **41**, 39-42. https://doi.org/10.1130/G33556.1
22. K. Yoshiya, Y. Sawaki, T. Shibuya, S. Yamamoto, T. Komiya, T. Hirata, and S. Maruyama, *Chem. Geol.*, 2015, **403**, 58-73. https://doi.org/10.1016/j.chemgeo.2015.03.007
23. Z. Lin, X. Sun, Y. Lu, H. Strauss, L. Xu, J. Gong, B. M. A. Teichert, R. Lu, H. Lu, W. Sun, and J. Peckmann, *Chem. Geol.*, 2016, **440**, 26-41. https://doi.org/10.1016/j.chemgeo.2016.07.007
24. M. Nishizawa, H. Yamamoto, Y. Ueno, S. Tsuruoka, T. Shibuya, Y. Sawaki, S. Yamamoto, Y. Kon, K. Kitajima, T. Komiya, S. Maruyama, and T. Hirata, *Geochim. Cosmochim. Ac.*, 2010, **74**, 2760-2778. https://doi.org/10.1016/j.gca.2010.02.014
25. N. S. Belshaw, X. K. Zhu, Y. Guo, and R. K. O'Nions, *Inter. J. Mass Spectrom.*, 2000, **197**, 191-195. https://doi.org/10.1016/S1387-3806(99)00245-6
26. S. Weyer and J. B. Schwieters, *Inter. J. Mass Spectrom.*, 2003, **226**, 355-368. https://doi.org/10.1016/S1387-3806(03)00078-2
27. N. Dauphas, P. E. Janney, R. A. Mendybaev, M. Wadhwa, F. M. Richter, A. M. Davis, M. Van Zuilen, R. R. Hines, and C. N. Foley, *Anal. Chem.*, 2004, **76**, 5855-5863. https://doi.org/10.1021/ac0497095
28. F. Poitrasson, A. N. Halliday, D.-C. Lee, S. Levasseur, and N. Teutsch, *Earth Planet. Sc. Lett.*, 2004, **223**, 253-266. https://doi.org/10.1016/j.epsl.2004.04.032
29. P. R. Craddock and N. Dauphas, *Geostand. Geoanal. Res.*, 2011, **35**, 101-123. https://doi.org/10.1111/j.1751-908X.2010.00085.x
30. I. C. Lyon, J. M. Saxton, and S. J. Cornah, *Inter. J. Mass Spectrom. Ion Process.*, 1998, **172**, 115-122. https://doi.org/10.1016/S0168-1176(97)00143-2
31. J. M. Huberty, N. T. Kita, R. Kozdon, P. R. Heck, J. H. Fournelle, M. J. Spicuzza, H. Xu and J. W. Valley, *Chem. Geol.*, 2010, **276**, 269-283. https://doi.org/10.1016/j.chemgeo.2010.06.012
32. N. T. Kita, J. M. Huberty, R. Kozdon, B. L. Beard and

J. W. Valley, *Surf. Interface Anal.*, 2011, **43**, 427-431. http://doi.org/10.1002/sia.3424

33. L. R. Riciputi, B. A. Paterson and R. L. Ripperdan, *Inter. J. Mass Spectrom.*, 1998, **178**, 81-112. https://doi.org/10.1016/S1387-3806(98)14088-5
34. J. Marin-Carbonne, C. Rollion-Bard, and B. Luais, *Chem. Geol.*, 2011, **285**, 50-61. https://doi.org/10.1016/j.chemgeo.2011.02.019
35. M. J. Whitehouse and C. M. Fedo, *Geology*, 2007, **35**, 719-722. https://doi.org/10.1130/G23582A.1
36. X.-Y. Zheng, B. L. Beard, S. Lee, T. R. Reddy, H. Xu, and C. M. Johnson, *Chem. Geol.*, 2017, **450**, 235-247. https://doi.org/10.1016/j.chemgeo.2016.12.038
37. T. Hirata and T. Ohno, *J. Anal. At. Spectrom.*, 2001, **16**, 487-491. http://doi.org/10.1039/B100946J
38. T. Hirata, Y. Hayano, and T. Ohno, *J. Anal. At. Spectrom.*, 2003, **18**, 1283-1288. http://dx.doi.org/10.1039/B305127G
39. T. Hirata and Y. Kon, *Anal. Sci.*, 2008, **24**, 345-353. http://doi.org/10.2116/analsci.24.345
40. J. Kosler, R. B. Pedersen, C. Kruber and P. J. Sylvester, *J. Anal. At. Spectrom.*, 2005, **20**, 192-199. http://doi.org/10.1039/B412169D
41. I. Horn, F. von Blanckenburg, R. Schoenberg, G. Steinhoefel, and G. Markl, *Geochim. Cosmochim. Ac.*, 2006, **70**, 3677-3688. https://doi.org/10.1016/j.gca.2006.05.002
42. G. Steinhoefel, I. Horn and F. von Blanckenburg, *Chem. Geol.*, 2009, **268**, 67-73. https://doi.org/10.1016/j.chemgeo.2009.07.010
43. M. Oeser, S. Weyer, I. Horn, and S. Schuth, *Geostand. Geoanal. Res.*, 2014, **38**, 311-328. https://doi.org/10.1111/j.1751-908X.2014.00288.x
44. F. Poitrasson and F.-X. d'Abzac, *J. Anal. At. Spectrom.*, 2017, **32**, 1075-1091. http://doi.org/10.1039/C7JA00084G
45. D. Malinovsky, A. Stenberg, I. Rodushkin, H. Andren, J. Ingri, B. Ohlander, and D. C. Baxter, *J. Anal. At. Spectrom.*, 2003, **18**, 687-695. http://doi.org/10.1039/B302312E
46. Z. Hu, Y. Liu, S. Gao, W. Liu, W. Zhang, X. Tong, L. Lin, K. Zong, M. Li, H. Chen, L. Zhou and L. Yang, *J. Anal. At. Spectrom.*, 2012, **27**, 1391-1399. http://doi.org/10.1039/C2JA30078H
47. M. Oeser, S. Weyer, I. Horn and S. Schuth, Geostand. *Geoanal. Res.*, 2014, **38**, 311-328. https://doi.org/10.1111/j.1751-908X.2014.00288.x
48. J. A. Schuessler and F. von Blanckenburg, *Spectrochim. Acta B*, 2014, **98**, 1-18. https://doi.org/10.1016/j.sab.2014.05.002
49. T. Luo, Z. Hu, W. Zhang, Y. Liu, K. Zong, L. Zhou, J. Zhang, and S. Hu, *Anal. Chem.*, 2018, **90**, 9016-9024. https://doi.org/10.1021/acs.analchem.8b01231
50. J. Lin, Y. Liu, Z. Hu, W. Chen, C. Zhang, K. Zhao, and X. Jin, *J. Anal. At. Spectrom.*, 2019, **34**, 1145-1153. http://doi.org/10.1039/C9JA00013E
51. X.-Y. Zheng, B. L. Beard, and C. M. Johnson, *J. Anal. At. Spectrom.*, 2018, **33**, 68-83. http://doi.org/10.1039/C7JA00272F
52. Y. -S. He, S. Ke, F. -Z. Teng, T. -T. Wang, H. -J. Wu, Y. -H. Lu, and S.-G. Li, *Geostand. Geoanal. Res.*, 2015, **39**, 341-356. https://doi.org/10.1111/j.1751-908X.2014.00304.x
53. K.-Y. Chen, H.-L. Yuan, P. Liang, Z.-A. Bao, and L. Chen, *Inter. J. Mass Spectrom.*, 2017, **421**, 196-203. https://doi.org/10.3969/j.issn.1007-2802.2016.03.010
54. Z. Hu, W. Zhang, Y. Liu, S. Gao, M. Li, K. Zong, H. Chen, and S. Hu, *Anal. Chem.*, 2015, **87**, 1152-1157. http://doi.org/10.1021/ac503749k
55. P. D. P. Taylor, R. Maeck, and P. De Bièvre, *Inter. J. Mass Spectrom. Ion Process.*, 1992, **121**, 111-125. https://doi.org/10.1016/0168-1176(92)80075-C
56. E. D. Young, A. Galy, and H. Nagahara, *Geochim. Cosmochim. Ac.*, 2002, **66**, 1095-1104. https://doi.org/10.1016/S0016-7037(01)00832-8
57. X. K. Zhu, Y. Guo, R. J. P. Williams, R. K. O'Nions, A. Matthews, N. S. Belshaw, G. W. Canters, E. C. de Waal, U. Weser, B. K. Burgess, and B. Salvato, *Earth Planet. Sc. Lett.*, 2002, **200**, 47-62. https://doi.org/10.1016/S0012-821X(02)00615-5
58. F.-X. d'Abzac, B. L. Beard, A. D. Czaja, H. Konishi, J. J. Schauer, and C. M. Johnson, *Anal. Chem.*, 2013, **85**, 11885-11892. http://doi.org /10.1021/ac402722t